



Cite this: *Dalton Trans.*, 2015, **44**, 10661

Received 10th December 2014,  
Accepted 19th January 2015

DOI: 10.1039/c4dt03780d

www.rsc.org/dalton

## Crystal and magnetic structures of the brownmillerite $\text{Ca}_2\text{Cr}_2\text{O}_5$

Angel M. Arevalo-Lopez and J. Paul Attfield\*

Powder neutron diffraction and magnetic susceptibility measurements at 10–300 K have been used to determine the crystal and magnetic structures of brownmillerite type  $\text{Ca}_2\text{Cr}_2\text{O}_5$ , which was obtained by reduction of the high pressure phase  $\text{CaCrO}_3$  through hard-soft chemistry. The ambient temperature crystal structure of  $\text{Ca}_2\text{Cr}_2\text{O}_5$  is refined in space group  $I2mb$  and the unusual tetrahedral coordination of  $\text{Cr}^{3+}$  results in local structural distortions.  $\text{Cr}^{3+}$  spins order antiferromagnetically below 220 K and a substantial observed canting of moments shows that Heisenberg exchange is weak or frustrated and competes with antisymmetric Dzyaloshinskii–Moriya interactions.

### Introduction

Metastable, perovskite-related oxides of transition metals in unusual oxidation states or coordination geometries offer new materials that may have useful magnetic or electronic properties.<sup>1</sup> We have recently used ‘hard-soft’ chemistry, in which the instability of a dense precursor prepared under ‘hard’ high pressure-temperature conditions is partially relieved through ‘soft’ post-synthesis modification, to synthesise new vacancy-ordered perovskite oxides.

Low-temperature hydrogen reductions of the cubic perovskite  $\text{SrCrO}_3$ , which requires synthesis pressures in excess of 4 GPa,<sup>2,3</sup> gave two new  $\text{SrCrO}_{3-\delta}$  phases with oxygen deficiencies  $\delta = 0.2$  and  $0.25$ .<sup>4</sup> These have complex superstructures due to oxide loss and reconstruction of widely-spaced cubic-(111) anion planes, which relaxes  $\text{Cr}^{4+}$  coordination from the octahedral geometry imposed at high pressure to tetrahedral. The  $\text{SrCrO}_{2.8}$  superstructure has subsequently been stabilised at ambient pressure by substitution of Fe for Cr.<sup>5</sup> The perovskite  $\text{SrCrO}_3$  and the reduced  $\text{SrCrO}_{2.8}$  structure were also stabilised epitaxially as thin films, with rapid oxygen uptake or loss on cycling between the two phases.<sup>6</sup>

The hard-soft route was also used to discover three reduced  $\text{CaCrO}_{3-\delta}$  phases.<sup>7</sup> The high pressure precursor  $\text{CaCrO}_3$  has an orthorhombically-distorted perovskite structure.<sup>8,9</sup> Reductions using a 90% Ar /10%  $\text{H}_2$  gas mixture at 400–450 °C revealed that three oxygen-deficient superstructure phases were formed, as shown in Fig. 1. The  $\text{CaCrO}_{3-\delta}$  perovskite superstructures are based on stacking of tetrahedral (T) and octahedral (O) layers, with increasing T/(T + O) ratio  $\delta = 0.33 \rightarrow 0.4 \rightarrow 0.5$  as

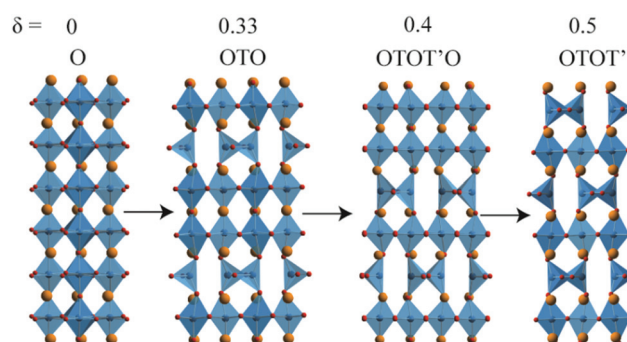


Fig. 1 Stacking sequences of octahedral (O) and tetrahedral (T) layers in the  $\text{CaCrO}_{3-\delta}$  series, where the final  $\delta = 0.5$  phase is the brownmillerite  $\text{Ca}_2\text{Cr}_2\text{O}_5$ .

reduction proceeds. This structural mechanism had not previously been reported for reduced ternary  $\text{ABO}_{3-\delta}$  perovskites but is found in  $\text{CaTi}_{1-x}\text{Fe}_x\text{O}_{3-x}$  where Fe-content determines the T/(T + O) layer ratio.<sup>10</sup> Magnetic ordering transitions were observed for the three reduced  $\text{CaCrO}_{3-\delta}$  phases at 150–200 K.<sup>7</sup>

The most reduced  $\text{CaCrO}_{3-\delta}$  phase,  $\text{Ca}_2\text{Cr}_2\text{O}_5$ , has a brownmillerite ( $\text{Ca}_2\text{Fe}_2\text{O}_5$ )<sup>11</sup> type structure where tetrahedral layers are stacked out-of-phase with their neighbours resulting in the OTOT' stacking sequence shown in Fig. 1. There is one prior report of a  $\text{Ca}_2\text{Cr}_2\text{O}_5$  brownmillerite prepared at ambient pressure,<sup>12</sup> but the structure was not characterized.  $\text{Ca}_2\text{Cr}_2\text{O}_5$  is notable as the brownmillerite structure contains  $\text{Cr}^{3+}$  in both octahedral and tetrahedral environments. The latter coordination is rare as crystal field effects provide strong stabilisation of  $\text{Cr}^{3+}$  in octahedral environments. The structure of  $\text{Ca}_2\text{Cr}_2\text{O}_5$  was refined in the aristotype  $Imma$  brownmillerite structure, in which the chains of tetrahedra in the T layers are disordered, as the X-ray data in the previous study were not

Centre for Science at Extreme Conditions (CSEC) and School of Chemistry, University of Edinburgh, Edinburgh, EH9 3FD, UK. E-mail: j.p.attfield@ed.ac.uk

sensitive to possible ordered superstructures.<sup>7</sup> Here we report a neutron diffraction study of  $\text{Ca}_2\text{Cr}_2\text{O}_5$  which has provided structural characterisation of the chain order, and has also enabled us to solve the low temperature magnetic order of  $\text{Cr}^{3+}$  spins.

## Experimental

$\text{CaCrO}_3$  precursors were synthesized from a stoichiometric mixture of  $\text{Ca}_3\text{Cr}_2\text{O}_8$  and  $\text{Cr}_2\text{O}_3$  in a multi-anvil Walker-type press at 9 GPa and 1100° C. A 90% Ar/10%  $\text{H}_2$  gas mixture was used to reduce  $\text{CaCrO}_3$  samples to  $\text{Ca}_2\text{Cr}_2\text{O}_5$ .

Magnetization data were measured on a Quantum Design MPMS SQUID magnetometer. Susceptibilities in zero field cooled (ZFC) and field cooled (FC) conditions were recorded in the 2–300 K temperature range with a 0.5 T applied field.

Time-of-flight neutron diffraction data were collected using the GEM diffractometer at the ISIS neutron facility. Several samples were combined in order to obtain a suitable amount for the experiment (~140 mg). Profiles were recorded at 10, 100, 200 and 300 K. Structural and magnetic models were fitted to data from banks 3, 4 and 5, centred respectively at  $2\theta = 35, 64$  and  $91^\circ$ .

## Results and discussion

### Crystal structure

No structural phase changes were observed between 10 and 300 K, and the crystal structure of  $\text{Ca}_2\text{Cr}_2\text{O}_5$  was refined using the 300 K neutron data. This structure was previously refined against X-ray data in the aristotype *Imma* brownmillerite structure, in which the tetrahedral are disordered.<sup>7</sup> Ordered tilts of the tetrahedra can give rise to low symmetry superstructures,<sup>13</sup> as found in other reported  $\text{Ca}_2\text{M}_2\text{O}_5$  brownmillerites at room temperature.  $\text{Ca}_2\text{Fe}_2\text{O}_5$  has a *Pnma* superstructure<sup>14</sup> while the high pressure phases  $\text{Ca}_2\text{Al}_2\text{O}_5$ <sup>15</sup> and  $\text{Ca}_2\text{Ga}_2\text{O}_5$ <sup>16</sup> have polar *I2mb* (a non-standard setting of *Ima2*) space group symmetry. A more complex *Pcmb* supercell with doubling of the *c*-axis parameter was recently reported in  $\text{Ca}_2\text{Co}_2\text{O}_5$ .<sup>17</sup> Fits of the two simple ordering models to the 300 K profile of  $\text{Ca}_2\text{Cr}_2\text{O}_5$  gave a slightly better goodness-of-fit  $\chi^2 = 1.63$  for *I2mb* than for *Pnma* where  $\chi^2 = 1.69$ , and no breaking of the body-centring reflection condition was observed. Hence the *I2mb* model is reported here as the ordered brownmillerite superstructure for  $\text{Ca}_2\text{Cr}_2\text{O}_5$  between 10 and 300 K, and this symmetry is corroborated by the analysis of structural parameters described below. Fits to the profiles are shown in Fig. 2, and refinement results are summarised in Tables 1 and 2.

Bond distances and angles for  $\text{Ca}_2\text{Cr}_2\text{O}_5$  in Table 2 allow a detailed analysis of the structural distortions. Bond valence sum (BVS)<sup>18</sup> values for the two Cr sites are consistent with the presence of  $\text{Cr}^{3+}$ , although the value for the Cr2 site is high, as often occurs for strained coordinations. The  $\text{Cr1O}_6$  octahedron is tetragonally distorted due to the structural connectivity, but

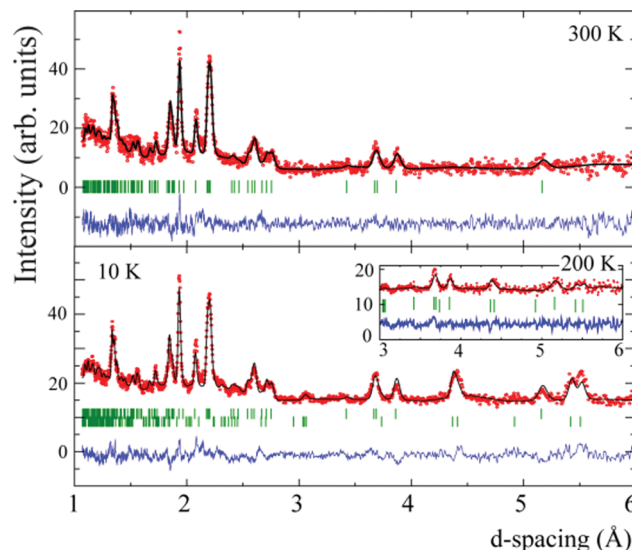


**Fig. 2** Rietveld fits to 300 K and 10 K GEM neutron diffraction patterns for  $\text{Ca}_2\text{Cr}_2\text{O}_5$ . Lower tickmarks in the 10 K pattern correspond to the magnetic phase with  $k = (111)$ . Data are from GEM bank 3, centred at  $2\theta = 35^\circ$ . The inset shows the region containing magnetic peaks in the 200 K profile.

**Table 1** Refined parameters for  $\text{Ca}_2\text{Cr}_2\text{O}_5$  in space group *I2mb* from the fit to 300 K neutron powder diffraction data<sup>a</sup>

Atom	Site	x	y	z
Ca	8c	0.497(3)	0.1074(4)	0.012(2)
Cr1	4a	0.501(4)	0.5	0.5
Cr2	4b	−0.007(4)	0.25	0.936(2)
O1	8c	0.754(2)	0.4919(5)	0.746(2)
O2	8c	0.022(2)	0.1398(3)	0.036(1)
O3	4b	0.162(2)	0.75	0.366(2)

<sup>a</sup> Cell parameters  $a = 5.420(4)$ ,  $b = 14.770(10)$ , and  $c = 5.509(4)$  Å; isotropic thermal parameter  $U_{\text{iso}} = 0.038(2)$  Å<sup>2</sup>; residuals  $R_{\text{wp}} = 0.066$  and  $R_p = 0.052$ .

**Table 2** Bond distances (Å), angles (°), and bond valence sums (BVS) for the Cr sites in  $\text{Ca}_2\text{Cr}_2\text{O}_5$  from refinement against 300 K diffraction data

Cr1–O1 × 2	1.93(2)	Cr2–O2 × 2	1.73(1)
Cr1–O1 × 2	1.94(2)	Cr2–O3	1.83(2)
Cr1–O2 × 2	2.08(1)	Cr2–O3	1.90(2)
BVS(Cr1)	3.02	BVS(Cr2)	3.36
O1–Cr1–O1 × 2	178.6(12)	O2–Cr2–O2	140.9(8)
O1–Cr1–O1 × 2	88.9(1)	O2–Cr2–O3 × 2	99.1(9)
O1–Cr1–O1	89.8(12)	O2–Cr2–O3 × 2	103.7(7)
O1–Cr1–O1	92.5(12)	O3–Cr3–O3	106.9(7)
O1–Cr1–O2 × 2	87.5(6)		
O1–Cr1–O2 × 2	88.2(6)	Cr1–O1–Cr1	172.5(5)
O1–Cr1–O2 × 2	91.7(6)	Cr1–O2–Cr2	154.3(6)
O1–Cr1–O2 × 2	92.6(6)	Cr2–O3–Cr2	131.2(10)
O2–Cr1–O2	173.9(15)		

O–Cr1–O angles are close to 90 or 180°. However, the  $\text{Cr2O}_4$  tetrahedron is highly distorted with Cr2–O distances of 1.73–1.90 Å and opening of the O2–Cr2–O2 angle to 141° while other bond angles lie in the range 99–107°. The corresponding



GaO<sub>4</sub> tetrahedron in isostructural Ca<sub>2</sub>Ga<sub>2</sub>O<sub>5</sub> is far less distorted, with Ga–O distances of 1.82–1.89 Å and O–Ga–O angles of 106–122°. As Cr<sup>3+</sup> and Ga<sup>3+</sup> have almost identical ionic radii (0.615 and 0.62 Å for octahedral coordination) this comparison suggests that the excess distortion of Ca<sub>2</sub>Cr<sub>2</sub>O<sub>5</sub> reflects the instability of tetrahedrally-coordinated Cr<sup>3+</sup>, as this cation generally has a strong preference for octahedral coordination which maximises crystal field stabilisation energy of the 3d<sup>3</sup> electronic configuration. The Ca<sup>2+</sup> site coordination is comparable to that in other brownmillerites,<sup>14–16</sup> with seven short Ca–O bonds in the range 2.43–2.62 Å while other Ca–O distances are >2.85 Å.

A previously reported study of multiple La<sub>1–x</sub>A<sub>x</sub>MnO<sub>2.5</sub> (A = Ca, Sr, Ba) brownmillerite compositions showed that the different structural phases fall into distinct regions on a plot of the tetrahedral layer separation (*b*/2), which has value 7.385 Å for Ca<sub>2</sub>Cr<sub>2</sub>O<sub>5</sub>, against the deviation of the tetrahedral chains from 180°. The latter angle is defined as 180°–(O3–O3–O3 angle) and takes value 50.3(7)° in the 300 K structure of Ca<sub>2</sub>Cr<sub>2</sub>O<sub>5</sub>. The point for Ca<sub>2</sub>Cr<sub>2</sub>O<sub>5</sub> lies within the domain of the *I2mb* superstructure on the reported structure map, corroborating the space group assignment from the comparison of neutron fits above.

### Magnetic structure

Magnetization measurements for the Ca<sub>2</sub>Cr<sub>2</sub>O<sub>5</sub> sample revealed a Curie tail at low temperatures and a trace of ferromagnetic material, as found in our previous study of CaCrO<sub>3–δ</sub> phases.<sup>7</sup> These impurity contributions were subtracted to yield the susceptibility shown in Fig. 3. A transition is apparent near 200 K with no divergence between ZFC and FC data, suggesting that the spin order is antiferromagnetic. The inverse susceptibility shows linear variation with temperature at 240–300 K, and a Curie–Weiss fit in this range gives a paramagnetic moment of 3.0 μ<sub>B</sub> and a Weiss temperature of θ = –460 K. These values are in keeping with antiferromagnetically

**Table 3** Irreducible representations and basis vectors of magnetic moments *m* for propagation vector (111) applied to the Cr cation positions in space group *I2mb*

Irreps	Basis vectors	<i>m<sub>x</sub>, m<sub>y</sub>, m<sub>z</sub></i>			
		(0, 0, 0)	(0, 1/2, 0)	(x, 1/4, z)	(x, 3/4, –z)
Γ <sub>1</sub>	Ψ <sub>1</sub>	1, 0, 0	–1, 0, 0	0, 1, 0	0, –1, 0
Γ <sub>2</sub>	Ψ <sub>2</sub>	1, 0, 0	1, 0, 0	1, 0, 0	1, 0, 0
	Ψ <sub>3</sub>			0, 0, 1	0, 0, –1
Γ <sub>3</sub>	Ψ <sub>4</sub>	0, 1, 0	0, –1, 0	1, 0, 0	–1, 0, 0
	Ψ <sub>5</sub>	0, 0, 1	0, 0, 1	0, 0, 1	0, 0, 1
Γ <sub>4</sub>	Ψ <sub>6</sub>	0, 1, 0	0, 1, 0	0, 1, 0	0, 1, 0
	Ψ <sub>7</sub>	0, 0, 1	0, 0, –1		

coupled Cr<sup>3+</sup> *S* = 3/2 spins (ideal paramagnetic moment 3.9 μ<sub>B</sub>), given the limited fitting range for the parameters.

Magnetic diffraction peaks were observed in neutron profiles collected at 10 to 200 K. These peaks are indexed by magnetic propagation vector *k* = (111) and the possible irreducible representations (irreps) and basis vectors for spin order with this vector applied to the *I2mb* space group are shown in Table 3.

Fits using a single basis vector for the spin order did not account well for the magnetic intensities. However, a good fit (as shown for the 10 K data in Fig. 2) is obtained using a combination of the basis vectors Ψ<sub>5</sub>(Γ<sub>3</sub>) and Ψ<sub>6</sub>(Γ<sub>4</sub>). These describe a *C<sub>y</sub>G<sub>z</sub>* antiferromagnetic order of spins, following standard convention for magnetic order in perovskites.<sup>20</sup> Although the Cr1 and Cr2 site moments are not symmetry-related, refining their spin components independently did not give a significantly improved fit over a model where their components were constrained to be the same, so the latter description was used as the final model. The *m<sub>y</sub>* and *m<sub>z</sub>* moment components at 10 K have values of 1.08(5) and 1.33(7) μ<sub>B</sub>, and the resultant moment is *m* = 1.7(1) μ<sub>B</sub>. Neutron diffraction shows that the Néel temperature for Ca<sub>2</sub>Cr<sub>2</sub>O<sub>5</sub> is >200 K (see inset to Fig. 2), and hence somewhat higher than the susceptibility features observed in Fig. 3. An estimate of *T<sub>N</sub>* ≈ 220 K is obtained by fitting the temperature variation of the moment in Fig. 4a with a critical law *m*(*T*) = *m*(0)[1 – (*T*/*T<sub>N</sub>*)]<sup>β</sup> for an exponent β ≈ 0.3, in keeping with theoretical models such as the three-dimensional XY magnet for which β = 0.34.

The magnetic structure of Ca<sub>2</sub>Cr<sub>2</sub>O<sub>5</sub> consists of antiferromagnetic planes of Cr1 and Cr2 moments as shown in Fig. 4b. Spins lie in the *bc*-plane and are tilted by 51(4)° from the *b*-axis. Neighbouring Cr1 and Cr2 spins connected through Cr1–O–Cr2 bridges are canted by ~100° suggesting that anti-symmetric Dzialoshinskii–Moriya exchange is significant, given the absence of a centre of symmetry or other symmetry relations between Cr1 and Cr2, and that Cr1–O–Cr2 Heisenberg exchange interactions are weak or frustrated. This reduction in the low temperature ordered moment of 1.7 μ<sub>B</sub> from the ideal value of 3 μ<sub>B</sub> for 3d<sup>3</sup> Cr<sup>3+</sup> is also consistent with some frustration in the spin order. Such spin canting is unusual in brownmillerites, as most have simple collinear antiferromagnetic structures with moments parallel to *a* or *b*.

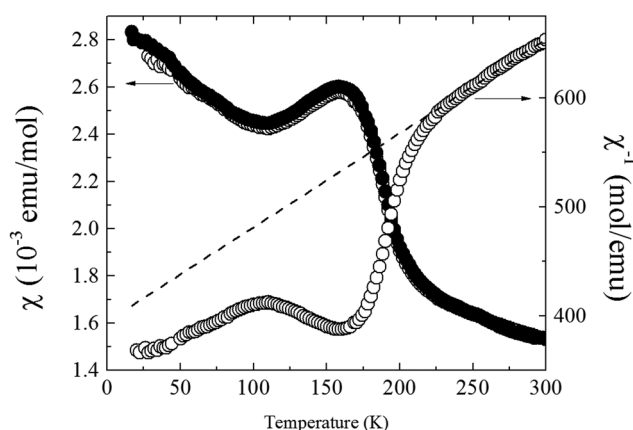


**Fig. 3** ZFC and FC magnetic susceptibilities for Ca<sub>2</sub>Cr<sub>2</sub>O<sub>5</sub>, and the inverse ZFC susceptibility showing a Curie–Weiss fit to the 240 < *T* < 300 K data.





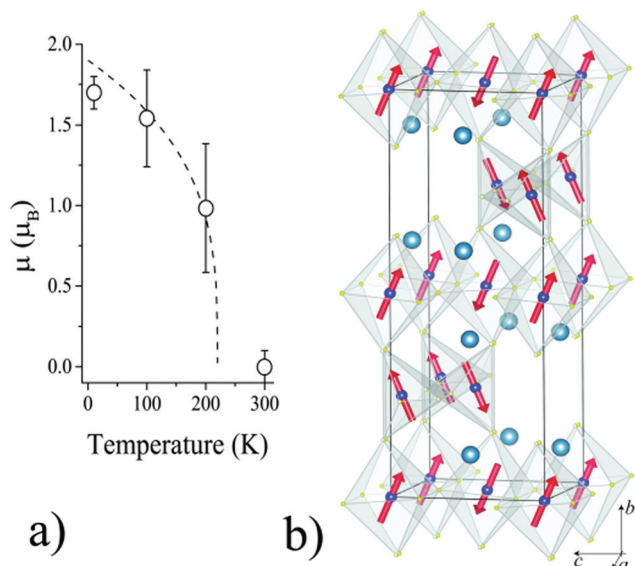


Fig. 4 (a) Temperature variation of the ordered Cr moment from neutron diffraction, showing the critical law fit described in the text. (b) Refined crystal and magnetic structure models for  $\text{Ca}_2\text{Cr}_2\text{O}_5$  showing the order of Cr spins in the  $bc$  plane.

## Conclusions

This study confirms that  $\text{Ca}_2\text{Cr}_2\text{O}_5$  synthesised by reduction of the high pressure perovskite phase  $\text{CaCrO}_3$  is a brownmillerite and adopts the ordered  $I2mb$  superstructure at ambient temperature. The unusual tetrahedral coordination of  $\text{Cr}^{3+}$  results in local structural distortions. The observation of  $\text{Cr}^{3+}$  in this unconventional environment illustrates the use of hard-soft chemistry to stabilise unusual coordination geometries. This brownmillerite material containing a high concentration of oxygen vacancies in cubic-perovskite (100) planes may offer high mobility for oxide ion transport, as was found in the hard-soft product  $\text{SrCrO}_{2.8}$ .<sup>4,6</sup> These stoichiometric reduced phases may also be useful model compounds to help understand oxide ion migration in chromium perovskite mixed conductors used in fuel cell anodes such as  $(\text{La}_{1-x}\text{Sr}_x)(\text{Cr}_{1-y}\text{M}_y)\text{O}_{3-\delta}$  ( $\text{M} = \text{Mn}, \text{Fe}, \text{Co}, \text{Ni}$ ).<sup>21</sup>

$\text{Ca}_2\text{Cr}_2\text{O}_5$  displays an antiferromagnetic spin ordering transition near 220 K, which is comparable to the 280 K Néel temperature for the perovskite  $\text{LaCrO}_3$ . Substantial canting of moments in successive layers is observed, suggesting that symmetric Heisenberg exchange interactions are weak or frustrated so that competing antisymmetric Dzyaloshinskii-Moriya interactions determine spin directions.

## Acknowledgements

We thank Dr I. da Silva (ISIS) and Dr Elise Pachoud (Edinburgh) for assistance with diffraction measurements. We also thank EPSRC, STFC and the Royal Society for support.

## Notes and references

- M. A. Hayward, *Semicond. Sci. Technol.*, 2014, **29**, 064010.
- A. J. Williams, A. Gillies, J. P. Attfield, G. Heymann, H. Huppertz, M. J. Martínez-Lopez and J. A. Alonso, *Phys. Rev. B: Condens. Matter*, 2006, **73**, 104409.
- L. Ortega-San-Martin, A. J. Williams, J. Rodgers, J. P. Attfield, G. Heymann and J. Huppertz, *Phys. Rev. Lett.*, 2007, **99**, 255701.
- A. M. Arevalo-Lopez, J. A. Rodgers, M. S. Senn, F. Sher, J. Farnham, W. Gibbs and J. P. Attfield, *Angew. Chem., Int. Ed.*, 2012, **51**, 10791.
- A. M. Arevalo-Lopez, F. Sher, J. Farnham, A. J. Watson and J. P. Attfield, *Chem. Mater.*, 2013, **25**, 2346.
- K. H. L. Zhang, P. V. Sushko, R. Colby, Y. Du, M. E. Bowden and S. A. Chambers, *Nat. Commun.*, 2014, **5**, 4669.
- A. M. Arevalo-Lopez, B. Liang, M. S. Senn, C. Murray, C. Tang and J. P. Attfield, *J. Mater. Chem. C*, 2014, **2**, 9364.
- M. A. Alario-Franco, E. Castillo-Martinez and A. M. Arevalo-Lopez, *High Pressure Res.*, 2009, **29**, 254.
- A. C. Komarek, S. V. Streltsov, M. Isobe, T. Moller, M. Hoelzel, A. Senyshyn, D. Trots, M. T. Fernandez-Diaz, T. Hansen, H. Gotou, T. Yagi, Y. Ueda, V. I. Anisimov, M. Gruninger, D. I. Khomskii and M. Braden, *Phys. Rev. Lett.*, 2008, **101**, 167204.
- Y. Bando, Y. Sekikawa, H. Yamamura and Y. Matsui, *Acta Crystallogr., Sect. A: Cryst. Phys., Diffr., Theor. Gen. Cryst.*, 1981, **37**, 723.
- E. F. Bertaut, P. Blum and A. Sagnieres, *Acta Crystallogr.*, 1959, **12**, 149.
- I. Kontoulis and B. C. H. Steele, *J. Eur. Ceram. Soc.*, 1992, **9**, 459.
- T. G. Parsons, H. D'Hondt, J. Hadermann and M. A. Hayward, *Chem. Mater.*, 2009, **21**, 5527.
- C. B. Vanpeteghem, R. J. Angel, J. Zhao, N. L. Ross, G. J. Redhammer and F. Seifert, *Phys. Chem. Miner.*, 2008, **35**, 493.
- V. Kahlenberg, R. X. Fischer and C. S. J. Shaw, *Am. Mineral.*, 2000, **85**, 1061.
- V. Kahlenberg and C. S. J. Shaw, *Z. Kristallogr.*, 2001, **216**, 206.
- J. Zhang, H. Zheng, C. D. Malliakas, J. M. Allred, Y. Ren, Q. Li, T. H. Han and J. F. Mitchell, *Chem. Mater.*, 2014, **26**, 7172.
- I. D. Brown and D. Altermatt, *Acta Crystallogr., Sect. B: Struct. Sci.*, 1985, **41**, 244.
- T. G. Parsons, H. D'Hondt, J. Hadermann and M. A. Hayward, *Chem. Mater.*, 2009, **21**, 5527.
- E. O. Wollan and W. C. Koehler, *Phys. Rev.*, 1955, **100**, 545.
- P. I. Cowin, C. T. G. Petit, R. Lan, J. T. S. Irvine and S. Tao, *Adv. Energy Mater.*, 2011, **1**, 314.

